Detailed description of the flow fields induced by a fire in a mechanically-ventilated compartment obtained using PIV

Lo c Perrin, Hajar Zaidaoui, Hugues Prétrel, Kevin Varral, Olivier Vauquelin

Detailed description of the flow fields induced by a fire in a mechanically-ventilated compartment obtained using PIV

Loïc Perrin[a,b], Hajar Zaidaoui[a], Hugues Prétrel[a*], Kevin Varral[b], Olivier Vauquelin[b]

[a] Institut de Radioprotection et de Sûreté Nucléaire (IRSN), PSN-RES/SA2I/LEF, Centre de Cadarache, 13115 Saint Paul Lez Durance, France, hugues.pretrel@irsn.fr

[b] Institut Universitaire des Systèmes Thermiques Industriels (IUSTI), UMR CNRS 7343, Aix Marseille Université, Technopôle de Château-Gombert, 13453 Marseille, France

*Corresponding author

Highlights:

- The feasibility of using PIV for compartment fires
- Global 2D flow fields in a mechanically-ventilated enclosure
- The effects of fire HRR on the flow field

Abstract:

This study analyses the performance of non-intrusive PIV (Particle Image Velocimetry) for the study of flows induced during a fire scenario in a mechanically-ventilated enclosure. PIV can be used to obtain detailed measurements for velocity fields in the enclosure and thus offer new experimental data for the understanding of the physical phenomena involved as well as to validate CFD simulation tools. The study is carried out on a reduced scale on an ethanol pool fire positioned in a ventilated enclosure. Several areas of interest are studied such as interaction between the fire plume and the ceiling, the flow under the ceiling and parietal flows. These zones can be analysed to obtain a picture of the global mean flow and associated velocity fields rarely reported in the literature. The influence of the fire heat release rate on the velocity fields is studied and highlights the design parameters.

Keywords: compartment fires; fluid dynamics, smoke management

1 Introduction

Compartment fires remain a major topic of interest in fire risk assessments in the industry and in the nuclear field in particular. The confinement of the fire source by the compartment leads to the accumulation of hot and toxic smoke in the room and thus to a significant coupling with the fire source. Furthermore, containment induces highly multidirectional flows with the rising smoke plume, interaction with the ceiling, the ceiling-jet and the return flow to the bottom of the room causing the room to fill with smoke. These fire scenarios are therefore complex to simulate and require advanced calculation tools such as CFD codes. For nuclear applications, the quantities of interest are notably the smoke temperatures that can lead to malfunctioning safety equipment and the concentrations of contaminated aerosols that may be released into the enclosure.

Measuring velocity fields is important in order to provide a database for simulation tools as well as to improve the understanding of physical phenomena. However, experimental databases including velocity fields remain limited due to the difficulty of implementing advanced measurement techniques on large-scale experiments involving fire. For fires in confined and ventilated environments, hostile environments, containment and the presence of soot are also considered. Under these conditions, obtaining experimental multidirectional velocity field data remains a challenge. Optical techniques such as particle imaging are rarely used for fire even though they could provide global measurements for multi-dimensional velocity fields. The velocity measurement techniques used in fire research remain basic and intrusive, limiting data production. In recent years, new non-intrusive techniques such as Particle Image Velocimetry (PIV) have been applied, mostly on small-scale experimental devices, to improve knowledge of velocity fields in fire scenarios.

PIV involves monitoring the displacement of tracer particles injected into a flow, assuming that their displacement is equal to that of the flow. During PIV, the particles are illuminated by a sheet of light generated by a laser and their displacement is evaluated by recording two successive images using cameras. As the time between the two images is known, the amplitude and direction of the particle velocity can be determined. Local measurements of instantaneous plane velocity components in the field of view can be obtained using specific image processing algorithms.

The first works involving PIV measurements for fire applications were carried out in the 1990s and focused on air entrainment flows in a near field pool fire [1] or inside the reactive zone [2]. PIV was later deployed to study free smoke flow at a doorway in order to better describe the flows of outgoing smoke and incoming fresh air [3], [4], [5], [6], [7]. Similar approaches were carried out on the more complex flows observed at a horizontal vent in order to evaluate models predicting outflow and inflow, but also to better characterise the oscillatory and chaotic regimes of these buoyant flows [8], [9]. PIV has also been used to assess the convective flow upstream of the propagation front in wildland fire applications [10], [11], to visualize vortex strength and the size of fire whirls [12] or to study flow in a large volume [13], [14]. For these applications, the flows were in an open environment with easy access and allowing for the effective implementation of PIV. Applications in closed rooms are more limited due to the complexity of implementation and the technical constraints inherent in accessibility and soot. Measurements have been taken in tunnels to study ceiling jet flows with natural ventilation in order to measure variation in the thickness of the smoke layer during propagation [15]. Attempts to describe the flows in a compartment have been proposed using maritime vessels to support the validation of simulation tools and using gas fires [16].

Studying flows in a compartment remains complex due to technical constraints and multidirectional flows. This study analyses the feasibility of applying PIV in a ventilated room in the configurations usually encountered at nuclear installations. It follows on from previous work showing feasibility for a controlled non-reactive electrical heat source that does not produce soot [17]. This study deals with the implementation of PIV in a configuration involving a pool fire in a mechanically-ventilated room. The objective is to identify the most appropriate technical settings for the use of PIV in this study configuration, to obtain new data characterising the mean

velocity fields and to highlight the influence of the fire power on this flow. The first part describes the experimental set-up and PIV method. The second part presents the results by focusing on the technical settings used, the global flow field and the influence of the fire power.

2 Material and Methods

2.1 Experimental set-up

The experiments are carried out using IRSN's reduced scale STYX system, which represents a ¼ scale reduction of a typical real enclosure for a nuclear facility. It consists of two superimposed rooms of 1.6 m^3 (1.6 m×1.0 m×1.0 m) and 1.0 m^3 (1.0 m×1.0 m×1.0 m). Each enclosure consists of a metal frame with insulating side wall panels (Monalite® calcium silicate plate with = 970 kg/m3, λ = 0.26 W/m K at 600°C). Only the lower room is considered in this study. The enclosure is mechanically ventilated by a network equipped with two fans located upstream and downstream of the enclosure. Due to technical constraints, the air supply and exhaust ducts are positioned within the enclosure. The air supply points are located in the lower part of the room. The air is injected towards the sidewalls to limit the impact on the fire. The extraction points are located in the upper part of the room. The positions of the ducts and the directions of the flows are shown in Fig. 1.

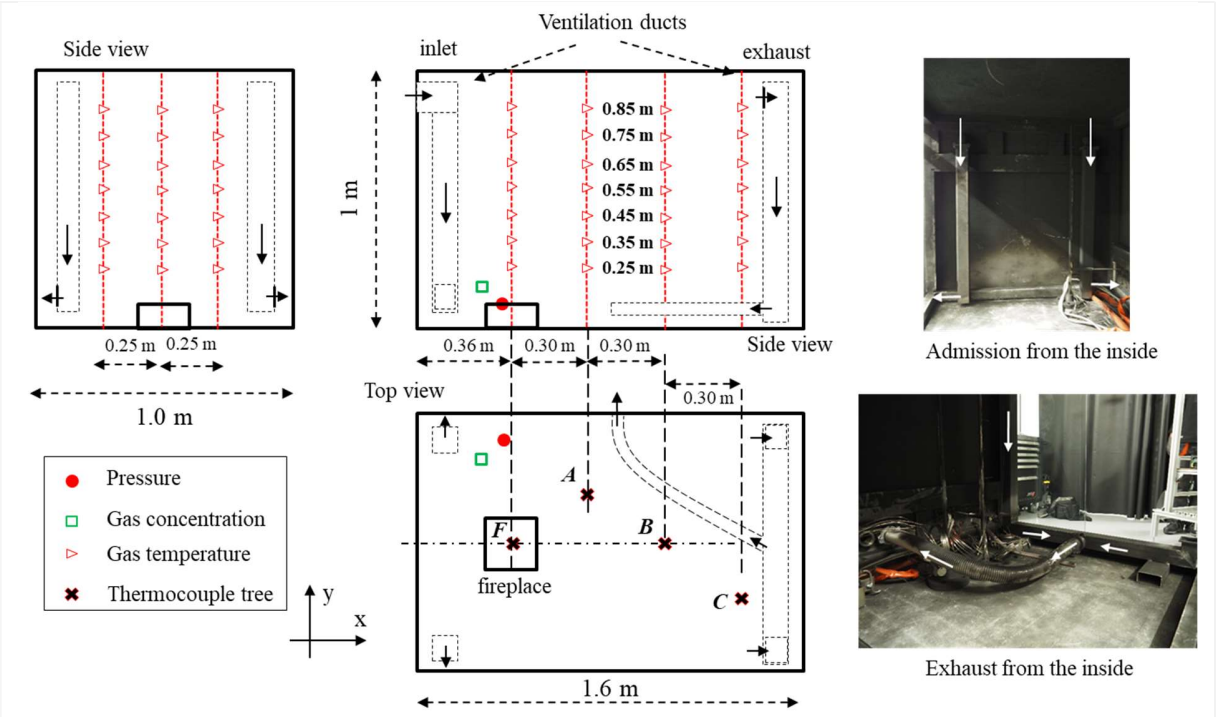

Fig. 1. Description of the experimental facility.

The fire is a pool fire comprising a circular Pyrex cup filled with liquid fuel. It is located on the floor and off-centre from one of the room's axes of symmetry for the purpose of investigating variation in the ceiling jet over a greater distance. Ethanol was selected because of its low

propensity to produce soot and thus limit deposits on the window, ensuring good optical access for PIV measurements by reducing the optical path length.

The experimental set-up was equipped with standard measuring devices for ventilation flowrates, vertical temperature profiles in the room and the concentration of chemical species: O_2, CO_2 and CO. The ventilation flowrates at the inlet and outlet were measured with orifice plates located upstream and downstream of the room and connected to pressure transducers. The temperature profiles were obtained using 0.5 mm diameter K-type thermocouples placed on four masts (A, B, C, F) distributed in the room as shown in Fig. 1. The concentration of chemical species was measured by an Emerson XSTREAM gas analysers sampling the gases in the lower part of the room. The pan was placed on a weighing device to measure the mass loss. The mass loss flow rate (MLR) was obtained by the time derivation of the mass signal.

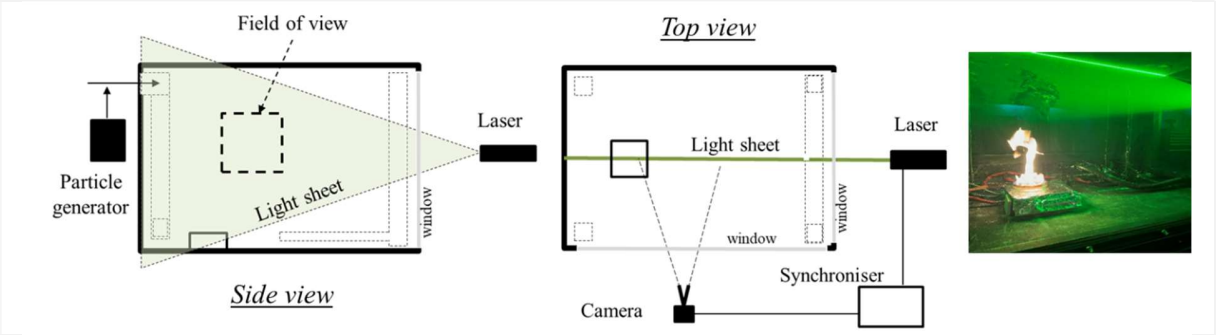

Fig. 2. Description of the set-up for the PIV system.

2.2 Description of the PIV system

A 2D PIV system was used to measure velocity fields in the median plane of the enclosure (see Fig. 2). The measuring equipment consists of a laser source, an olive oil droplet generator, a CCD camera and a synchroniser for coupling between the laser and the camera. The light source used is a pulsed Nd-YAG laser (Quantel EverGreen² YAG200-15-QTL) with a power of 200 mJ/pulse set at a maximum frequency of 15 Hz (or 7.5 Hz for a pair of images). It can generate two laser pulses at a wavelength of 532 nm, with a duration of 5 ns and separated by a lapse of time (dt) fixed by the operator according to the flow velocity. The laser beams are spread into a sheet using a cylindrical lens with an estimated thickness of less than 4 mm. The CCD camera (630091 PowerView, 2,048 x 2,048 resolution), equipped with a 50 mm focal length and a passband filter centred on the laser wavelength, is positioned perpendicular to the light sheet outside the room at a distance of between 0.3 m and 0.75 m from the window, depending on the size of the field of view required. Two of the room walls were replaced with standard glass panels to ensure optical accessibility. The field of view of the camera was spatially calibrated with a calibration plate. Images were captured (including laser-camera synchronization) and processed using INSIGHT4G software. In order to obtain local measurements for the flow velocity components, captured images are split into smaller square Interrogation Areas (IA), to which a cross-correlation algorithm is applied. IA are either 32 or 64 pixels wide and benefit from 50% overlap, allowing to reach a resolution of 1.67 mm for a 210 mm x 210 mm field of view and 2.84 mm for a 358 mm x 358 mm one. The olive oil droplets were injected with a

generator (model 9307-6) into the inlet duct upstream of the flowrate measurement in order to avoid an additional air flow. The particle size, between 0.5 and 3 µm, met the flow tracking criterion.

2.3 Test grid and protocol

The study focuses on the detailed description of the flow in a fire in a closed, mechanically-ventilated room. For this purpose, a given ventilation configuration was defined with a ventilation flow rate of 30 m^3/h, which corresponds to an ACH (Air Change rate per Hour) of 20 h^{-1}. Study parameters cover the investigated area and the fire heat release rate (HRR). Due to the limited size of the camera measurement areas, several investigation zones were selected to cover ceiling plume interaction, ceiling flow and sidewall flow, named A, B, C, D, E and F as illustrated on Fig. 3. The six zones were studied for a given pool diameter of 0.12 m. For zones A, B and D' only, the effect of the fire HRR was quantitively studied by measuring two other pool diameters of 0.15 m and 0.205 m. The pool was made in borosilicate glass with a height of XX, YY, ZZ pour the pool diameters 0.12, 0.15 and 0.205 respectivelly. For each HRR, the experiment is repeated several times, without PIV with conventional measurements only, then with PIV for the different study areas. The camera position was changed for each study area and the calibration process was repeated. The duration of the fire is defined to obtain a combustion phase lasting approximately 30 to 40 minutes. The PIV measurements correspond to an acquisition period ranging from 40 seconds to 2 minutes over the stationary period of the experiment (see Fig. 4).

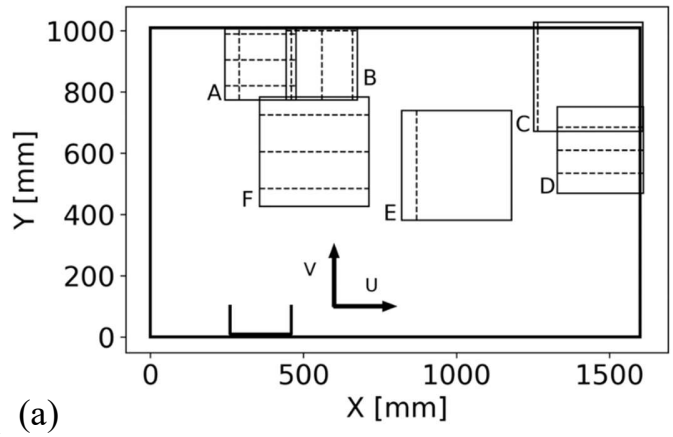

zone	Centre position [mm]			Side length [mm]
	X	Y	Z	
A	360	890	500	232
B	560	890	500	232
C	1430	850	500	355
D	1470	610	500	282
E	1000	560	500	358
F	535	605	500	358
D'	1430	648	500	210

(b)

Fig. 3. (a) Schematic diagram showing the positions of the investigated areas (A, B, C, D, E and F) and the locations of the profiles discussed in the analysis, (b) table of position and side length of the investigated areas (A, B, C, D, E, F and D').

3 Results

3.1 Description of the fire scenarios

Prior to the analysis of the velocity fields, changes in standard quantities are analysed from Fig. 4 where variation in the ventilation flowrate, mass of fuel and the temperature on the B-mast are

shown as examples. The ventilation flowrate is constant over time. The fuel mass decreases linearly with time leading to MLR constant over time. The mean values are 0.11 g/s, 0.18 g/s and 0.37 g/s for the three pool diameters, which leads to fire HRR of 3.2 kW, 5.2 kW, and 10 kW considering an effective combustion enthalpy of 28 MJ/kg [18]. The temperature initially increases rapidly and then reaches a steady state. Due to the high ventilation rate, oxygen concentrations decrease, but only slightly, maintaining the well-ventilated combustion regime. The temperature profile in the room shows vertical stratification characterised by a constant gradient typical of thermal stratification in confined spaces. The vertical temperature profiles show larger amplitudes for higher fire HRR.

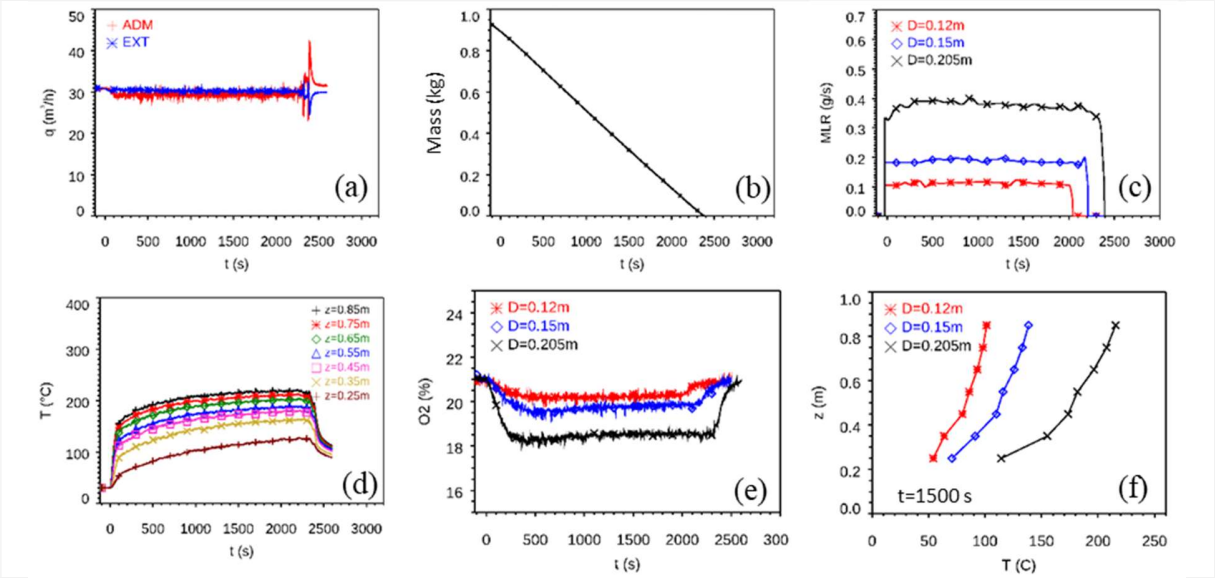

Fig. 4. Description of the tests with ethanol pool fire: (a) ventilation flowrates versus time for D=0.205 m, (b) fuel mass versus time for D=0.205 m, (c) MLR versus time for the three pool diameters (d) temperature on mast B versus time, for D=0.205 m, (e) O2 concentration versus time for the three pool diameters (f) Vertical temperature profile on mast B at t=1500 s for the three pool diameters.

3.2 PIV optimisation

The PIV measurements required adjustments to the experimental protocol and test conditions in order to satisfactorily validate the cross-correlation of the images. The main adverse effect is the presence of soot, which contributes on the one hand to reducing the homogeneity of the intensity of the laser sheet and on the other hand favours deposition on the glass walls.

The fuel producing the least soot was initially selected. Tests were carried out with dodecane liquid and propane gas leading to soot deposits on the glass walls and thus limiting the quality of the images. The best results were obtained with ethanol because of its low soot production.

Furthermore, a convergence study was carried out to evaluate the number of image pairs required to obtain converged mean values. On a given test configuration (D = 0.12 m) and profile (zone A, X = 289 mm), the convergence study shows that 300 image pairs are sufficient to obtain a

converged mean value of the horizontal and vertical velocity's components, respectively noted U and V (see Fig. 5). This result is in agreement with other similar studies [17]. However, the adequate number of pairs might increase with the proximity and diameter of the pool fire.

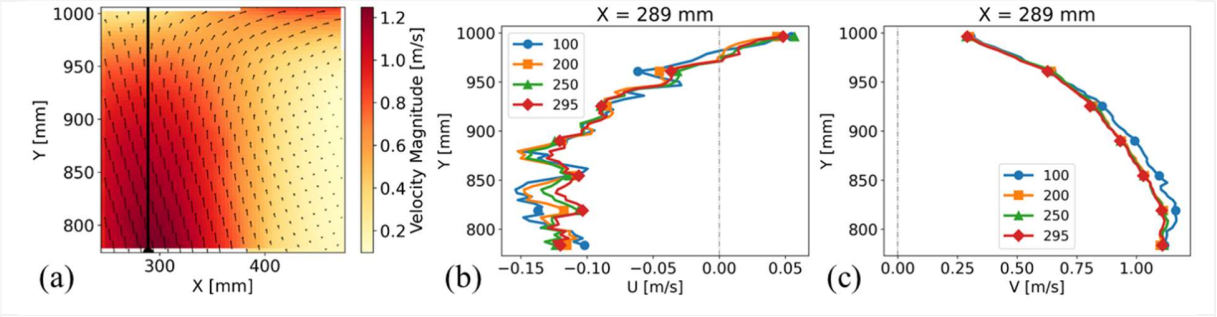

Fig. 5. Illustration of the convergence study regarding the number of images (zone A, D=0.12 m). (a) Velocity and vector field, (b) mean vertical profile (X=289 mm) of the horizontal U-component of the velocity for increasing number of averaged image pairs, (c) mean vertical profile (X=289 mm) of the vertical V-component of the velocity for increasing number of averaged image pairs.

In addition, the images were acquired over a period of a few seconds during the stationary phase. The influence of the acquisition period was evaluated by comparing the profiles obtained at four successive times over the quasi-stationary period. An example is shown in Fig. 6 by comparing the vertical profiles of the U and V-components from zone A for a 0.12 m pan. The differences related to the acquisition period remain negligible compared to the overall variations in the flow.

Therefore, in the following analysis, the presented results are mean values over one sequence of 300 image pairs. Exception made for results associated with D=0.205 m pool fire, who are obtained from sequences of 1000 images pairs.

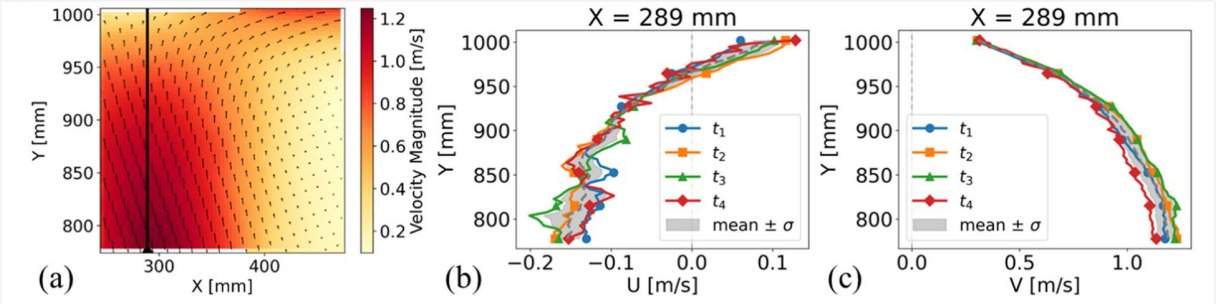

Fig. 6. Effects of the acquisition period on a given velocity profile (zone A, D=0.12 m). (a) Velocity and vector field, (b) mean vertical profile (X=289 mm) of the U-component at various periods, (c) mean vertical profiles (X=289 mm) of the V-component at various periods.

3.3 Characterisation of the flow field for a given configuration

The flow field is initially characterised in a given configuration with a pool diameter of 0.12 m. An overview of the flows in the enclosure is proposed based on streamlines calculated from the velocity field measured in each zone (A, B, C, D, E and F) (Fig. 7). A large eddy is thus observed, as induced by the fire and the plume flow interacting with the ceiling and the vertical sidewall. This eddy contributes to feeding the lower part of the room with smoke and bringing smoke back to the centre of the room. This overview shows the coherence of the PIV measurements taken in each zone in a new experiment and thus the possibility of reconstituting a global velocity field. While the plume flow and the ceiling jet have been extensively studied, very little research has been done on the downward flow at the walls which brings smoke to the lower part of the room. The PIV measurements presented here provide a detailed description of this flow in term of directions and amplitudes. This flow contributes to polluting the lower zone and thus to homogenising the gases in the room. We also note the upward return flow that will bring part of the smoke back towards the centre of the room. This large eddy certainly influences the vertical stratification of the smoke. The regular observation of vertical temperature profiles with a constant gradient in compartmented fires can be explained by this eddy circulation pattern. It is also likely that this type of phenomenon occurs as a function of the fire heat release rate, the height and width of the enclosure. This phenomenon can be compared to "overturning", reported in studies regarding the transient filling process of an enclosure [19], [20].

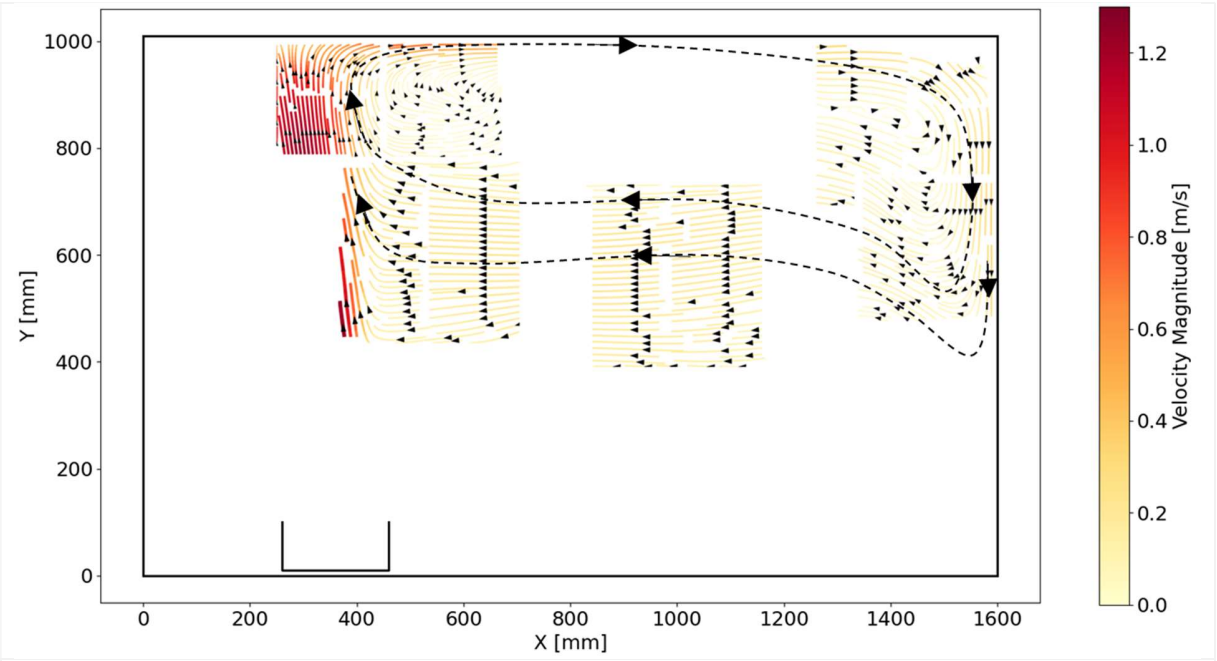

Fig. 7. Overview of the velocity field in the room (D = 0.12 m).

Each zone is then analyzed in independently.

Fig. 8 shows a vector field and the streamlines as well as the profiles of the vertical V and horizontal U-components of the velocity for zone A. The 2D velocity field shows the

deceleration of the upward flow of the plume as it approaches the ceiling followed by a radial flow away from the plume axis. The PIV measurements show a clear pattern in the flow field. The V-component decreases as it approaches the ceiling until it reaches zero at the stagnation point. The vertical profile of the V-component decelerates from about 1.25 m/s until 0. The horizontal profiles of the V-component show a typical gaussian shape peaking on the plume axis and decreasing towards the outside of the plume. The amplitude of the profiles decreases when approaching the ceiling. The radial flow results in an increase in the horizontal component away from the plume axis. This effect results in an increase in the U-component from the plume axis outwards to a maximum value of 0.6 m/s. It is important to note that the streamlines show a slight inclination of the plume axis. This effect is explained by the proximity of the fire to one of the sidewalls of the enclosure inducing a coanda-like phenomenon.

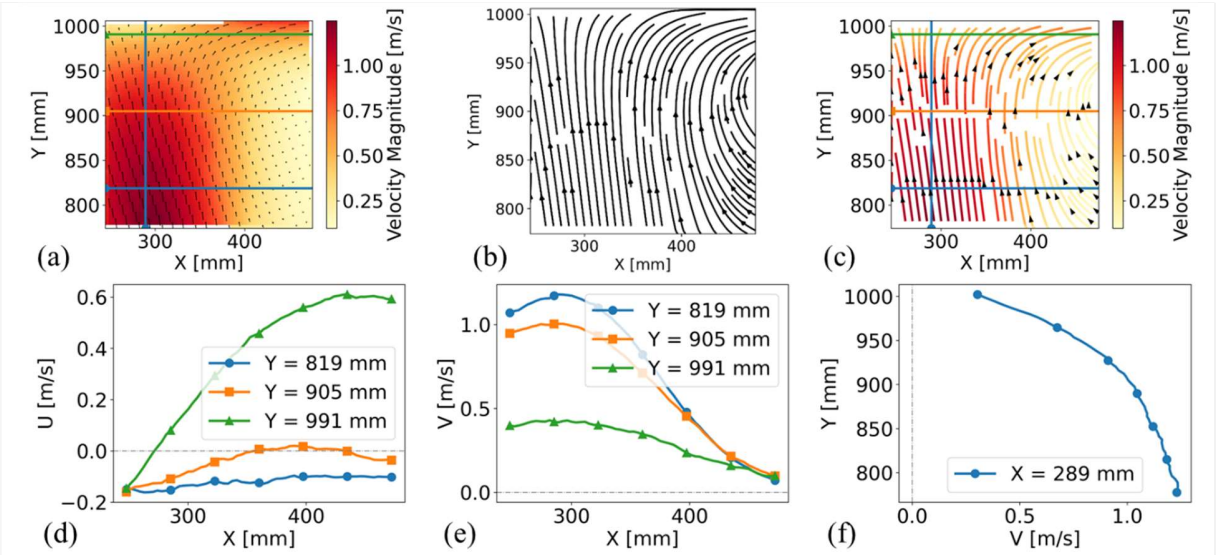

Fig. 8. Velocity field in the plume and ceiling jet interaction region (region A, D = 0.12 m). (a) Velocity field, vector field and locations of the profiles, (b) streamlines, (c) streamlines, velocity field and locations of the profiles, (d) mean horizontal profiles of the U-component for various Y locations, (e) mean horizontal profiles of the V component for various Y locations, (f) mean vertical profile of the V-component for X=289 mm.

The ceiling flow is then studied over zone B and the results are presented in Fig. 9. The ceiling flow is a horizontal radial flow with a maximum velocity close to the ceiling. The vertical profiles perpendicular to the flow direction of the U-component peak near the wall and then progressively decrease with distance from the wall. In our application, the spatial resolution is too coarse to determine the location of the boundary layer. The shape of the vertical profile of the U-component is similar regardless of horizontal position. Only the maximum amplitude decreases with distance from the plume axis (from 0.8 m/s to 0.6 m/s over about 0.2 m) due to

friction at the ceiling and the entrainment of air in the lower part of the flow. The thickness of the ceiling jet is about 50 mm. Thickening due to air entrainment over the distance considered is not significant.

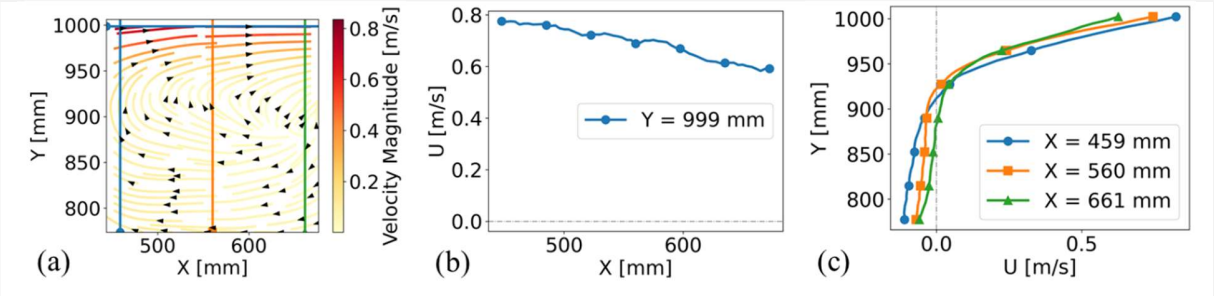

Fig. 9. Velocity field in the ceiling jet region (region B, D = 0.12 m). (a) Streamlines, velocity field and locations of the profiles, (b) mean horizontal profile of the U-component for Y=999 mm, (c) mean vertical profiles of the U-component for various X locations.

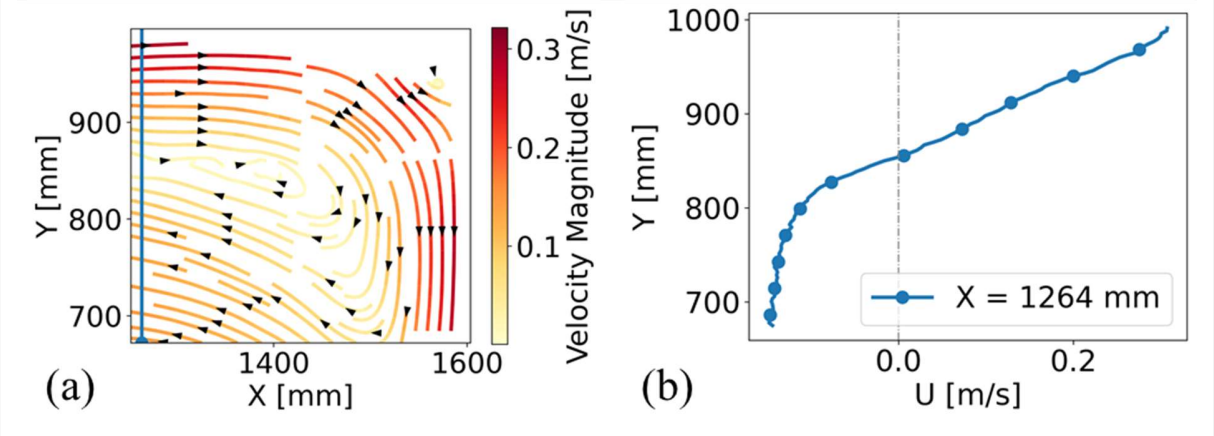

Fig. 10. Velocity field in the upper corner region (region C, D = 0.12 m). (a) Streamlines, velocity field and location of the profile, (b) mean vertical profile of the U-component for X=1264 mm.

The radial flow under the ceiling changes direction as it reaches the opposite side wall inducing acceleration on contact with the wall and then a parietal downward flow (Fig. 10). The streamlines show the presence of a larger eddy with the flow rising towards the central area of the room. The vertical profile of the U-component can be used to evaluate the thickness of the ceiling jet, which in this case is about 200 mm, thus confirming the thickening of the ceiling jet flow due to air entrainment.

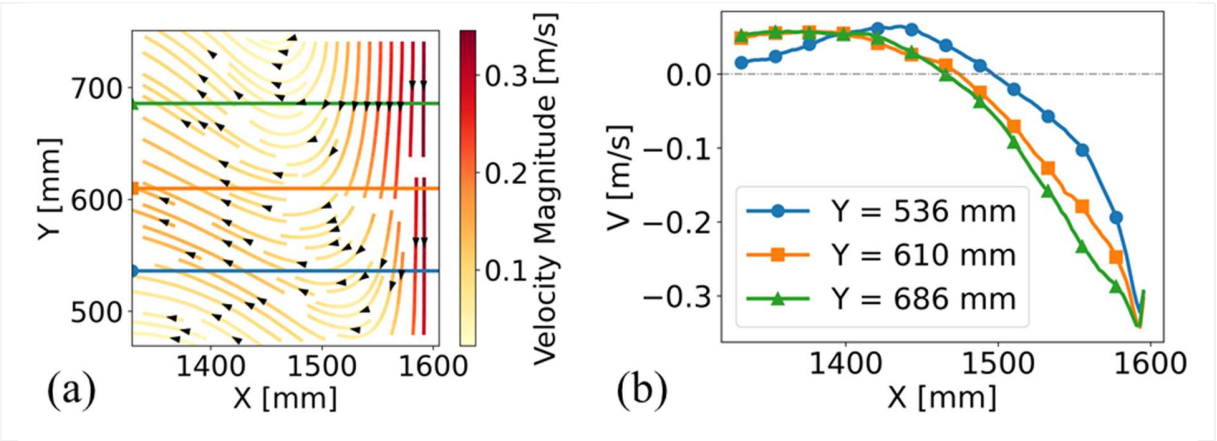

Fig. 11. Velocity field along the sidewall (region D, D = 0.12 m). (a) Streamlines, velocity field and locations of the profiles, (b) mean horizontal profile of the V-component for various Y locations.

Measurements in zone D confirm this parietal flow and the return flow towards the centre of the part probably induced by the buoyancy forces generated by the temperature of the flow (Fig. 11). The profile perpendicular to the flow direction of the V-component shows a similar shape to that observed for the ceiling jet for the U-component peaking close to the wall. However, the amplitude is lower in this case with values of approximately 0.3 m/s. The pattern whereby the downward and return flow to the centre of the room probably carries smoke and thus contributes to polluting the lower zone of the room is of interest. This large eddy may provide an explanation for the particular thermal stratification (reported in Fig. 4) often encountered in ventilated enclosures characterised by a constant gradient rather than a profile with two homogeneous zones [21].

Measurements in the centre of the room (zone E) confirm the return flow feeding the centre of the room (Fig. 12). The area selected is characterised by a horizontal flow in the direction of the fire and corresponds to part of the large eddy identified throughout the room. The vertical profile of the U-component shows an inflection confirming the result of a flow coming from the right and not simply a current generated by the plume entrainment.

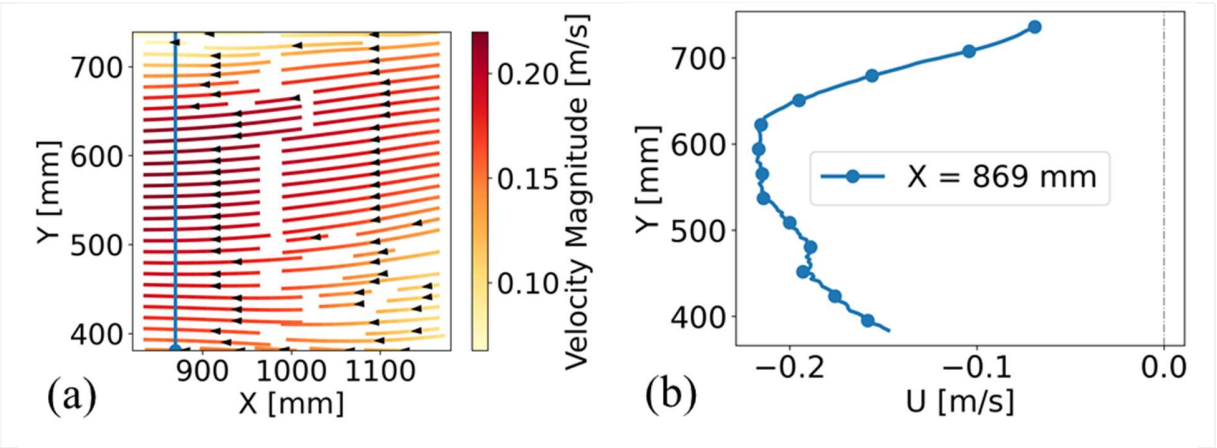

Fig. 12. Velocity field at the centre of the room (region E, D = 0.12 m). (a) Streamlines, velocity field and location of the profile, (b) mean vertical profile of the U component for X=869 mm.

Finally, measurements are taken in the region close to the plume (region F). The horizontal flow, previously reported in region E is observed again in region F directed at low speed towards the plume and is then drawn into it creating the vertical plume (Fig. 13). The horizontal profiles of the U and V components show the low amplitude of the horizontal flow (about 0.15 m/s) and the acceleration in the plume (V speed of about 1.2 m/s).

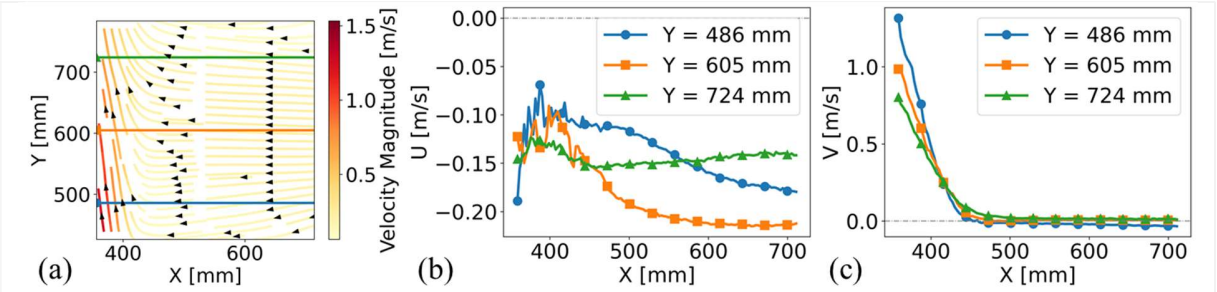

Fig. 13. Velocity field near the vertical plume (region F, D = 0.12 m). (a) Streamlines, velocity field and location of the profile, (b) mean horizontal profiles of the U component for various Y locations, (c) mean horizontal profiles of the V component for various Y locations.

3.4 The effects of the pool diameter on the velocity fields

The influence of the pool diameter and thus of the fire heat release rate is investigated for three profiles in regions A, B and D' (Fig. 14). As expected, the increase in HRR contributes to an increase in the amplitude of the flows

For the thermal plume, the vertical velocities are higher and the plume diameter larger with increasing fire HRR. The increase in fire HRR also appears to move the maximum velocity and thus reduce the plume tilt observed for D=0.12 m. The increase in HRR for the ceiling jet flow and the downward flow along the sidewall mainly increases amplitudes, but the shapes of the profiles remain unchanged.

Normalization is attempted by considering the ratio U^*/Q^{*n} with the dimensionless velocity $U^* = u/\sqrt{gH}$ and $V^* = V/\sqrt{gH}$ and the dimensionless fire HRR $Q^* = Q/\left(\rho C_p T\sqrt{g}H^{5/2}\right)$. For the thermal plume and ceiling jet, the exponent proposed by the theory is 1/3 [22].

When normalised with n=1/3, the profiles for the three diameters coincide, as shown in Fig. 14. Concerning the plume flow (see Fig. 14 (a) and Fig. 14 (b), while the profiles for the diameters 0.12 m and 0.15 m coincide perfectly, the profile for the highest HRR (D=0.205 m) shows an increased radial deceleration on the side closest to the wall. Normalising the ceiling jet (see Fig. 14 (c) and Fig. 14 (d) provides an excellent representation of the fire HRR with n=1/3 and is thus in very good agreement with the theoretical approaches. For the downward flow (see Fig. 14 (e) and Fig. 14 (f), the staggering of the profiles does not allow such appropriate normalization for all three profiles and none has been proposed in the literature. But normalization with n=1/3 remains effective for the parts of the profiles closest to the wall for diameters 0.12 m and 0.15 m. This normalization process suggests that the entire flow can be normalised, and not just individual flows such as the plume or ceiling jet. The fact that the factor n can vary in the volume of the enclosure can be used to reflect the specificities of certain zones.

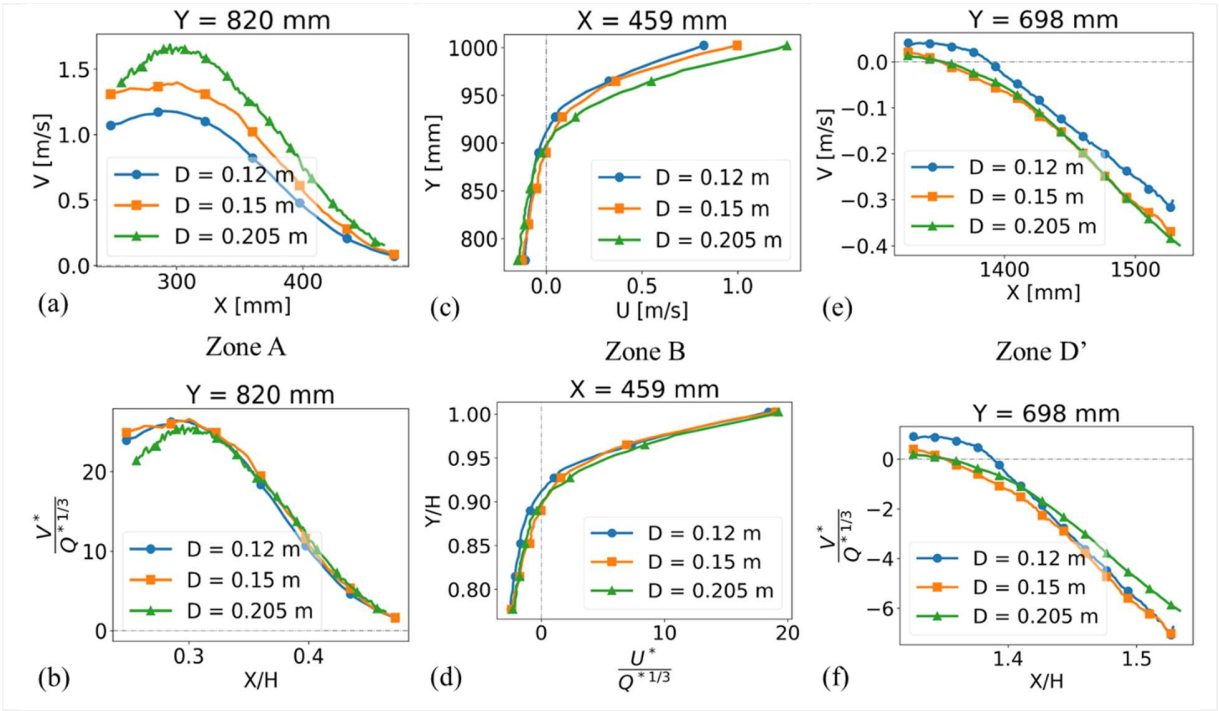

Fig. 14. The effects of the pool diameter on velocity profiles in regions A, B and D. (top line, velocity amplitude, (bottom line) velocity normalization. (a) V component horizontal profiles (zone A, Y=820 mm) for various pool diameters, (b) normalized V component horizontal profiles (zone A, Y=820 mm) for various pool diameters, (c) U component vertical profiles (zone B, X=459 mm) for various pool diameters, (d) normalized U component vertical profiles (zone B, X=459 mm) for various pool diameters, (e) V component horizontal profiles (zone D', Y=698 mm) for various pool diameters, normalized V component horizontal profiles (zone D', Y=698 mm) for various pool diameters.

4 Conclusions

The objective of this study was to evaluate the feasibility of experimentally measuring the velocity fields observed in a mechanically-ventilated enclosure in the presence of a fire source. Small-scale experiments were carried out on a 1.6m^3 device with ethanol pool fires. A Particle Image Velocimetry (PIV) system was set up to obtain 2D velocity field measurements in the median plane of the enclosure. The following conclusions were reached.

PIV is suitable for measuring the flows induced during a fire in a mechanically-ventilated enclosure. Selecting a fuel that produces little soot is recommended in order to avoid soot disturbing the optical access necessary for PIV.

The mean global velocity field in steady state conditions was reconstructed using the measurements taken in the different areas of the enclosure. A large eddy was identified formed by the thermal plume induced by the fire, its impact on the ceiling and then on the sidewall, allowing smoke to flow initially under the ceiling and then be partially transported to the lower part of the room. This downward flow, which is rarely considered in the literature, has been highlighted thanks to PIV. These new data allow us to propose explanations for the vertical temperature profiles observed in mechanically-ventilated enclosures.

The influence of fire HRR on the velocity fields was evaluated by experiments with several pool sizes. The increase in HRR leads to an increase in the amplitude of the velocities without modifying the structure of the flows. An attempt to normalise the velocity by the power is proposed and shows the generic feature of the global flow field based on the ratio U^*/Q^{*n}.

References

[1] X. C. Hou, J. P. Gore, and H. R. Baum, "Measurements and prediction of air entrainment rates of pool fires," *Symp. Combust.*, vol. 26, no. 1, pp. 1453–1459, 1996, doi: 10.1016/S0082-0784(96)80366-3.

[2] S. R. Tieszen, T. J. O'Hern, R. W. Schefer, E. J. Weckman, and T. K. Blanchat, "Experimental study of the flow field in and around a one meter diameter methane fire," *Combust. Flame*, vol. 129, no. 4, pp. 378–391, 2002, doi: 10.1016/S0010-2180(02)00352-8.

[3] R. Bryant, "The application of stereoscopic PIV to measure the flow of air into an enclosure containing a fire," *Exp. Fluids*, vol. 47, no. 2, pp. 295–308, 2009, doi: 10.1007/s00348-009-0656-z.

[4] R. Bryant, "A comparison of gas velocity measurements in a full-scale enclosure fire," *Fire Saf. J.*, vol. 44, no. 5, pp. 793–800, 2009, doi: 10.1016/j.firesaf.2009.03.010.

[5] A. Koched, H. Prétrel, O. Vauquelin, and L. Audouin, "Experimental determination of the discharge flow coefficient at a doorway for fire induced flow in natural and mixed convection," *Fire Mater.*, vol. 40, no. 1, pp. 114–128, 2016, doi: 10.1002/fam.2272.

[6] A. Koched, H. Prétrel, O. Vauquelin, and L. Audouin, "Measurement of turbulence statistics in compartment fire using stereoscopic PIV," in *18th International Symposium on the Application of Laser and Imaging Techniques to Fluid Mechanics*, 2016.

[7] A. Pearson, J. M. Most, and D. Drysdale, "Behaviour of a confined fire located in an unventilated zone," *Proc. Combust. Inst.*, vol. 31 II, pp. 2529–2536, 2007, doi: 10.1016/j.proci.2006.08.019.

[8] K. Varrall, H. Prétrel, S. Vaux, and O. Vauquelin, "Stereoscopic particle image velocimetry investigations of the mixed convection exchange flow through a horizontal vent," *Exp. Fluids*, vol. 58, no. 10, p. 151, Oct. 2017, doi: 10.1007/s00348-017-2434-7.

[9] P. Becerra-Barrios, K. Varrall, H. Prétrel, S. Vaux, and O. Vauquelin, "Experiments on

bidirectional flow through a ceiling vent in natural ventilation," in *1st Franco-AMSUD Energy and Environment Meeting Marseille, France, March 18-21, 2019*, 2019, pp. 1–6.

[10] F. Morandini, X. Silvani, D. Honoré, G. Boutin, A. Susset, and R. Vernet, "Slope effects on the fluid dynamics of a fire spreading across a fuel bed: PIV measurements and OH chemiluminescence imaging," *Exp. Fluids*, vol. 55, no. 8, 2014, doi: 10.1007/s00348-014-1788-3.

[11] A. Desai, S. Goodrick, and T. Banerjee, "Investigating the turbulent dynamics of small-scale surface fires," *Sci. Rep.*, vol. 12, no. 1, pp. 1–19, 2022, doi: 10.1038/s41598-022-13226-w.

[12] M. Shinohara, "Vortex strength and size of fire whirls without flames around a long narrow fire source," *Fire Saf. J.*, vol. 129, no. February, p. 103561, 2022, doi: 10.1016/j.firesaf.2022.103561.

[13] B. Giachetti, D. Couton, and F. Plourde, "Smoke spreading analysis from an experimental subway scale model," *Fire Saf. J.*, vol. 86, no. April, pp. 75–82, 2016, doi: 10.1016/j.firesaf.2016.10.001.

[14] I. Horváth, J. Van Beeck, and J. Buchlin, "Large-Scale Particle Image Velocimetry on a Full-Scale Pool Fire Large-Scale Particle Image Velocimetry on a Full-Scale Pool Fire 1 Introduction The application of PIV measurements on Fire and consequently where ambient light is inevitable is introduced ," in *16th Int Symp on Applications of Laser Techniques to Fluid Mechanics Lisbon, Portugal, 09-12 July, 2012*, 2012.

[15] Y. Oka, H. Oka, and O. Imazeki, "Ceiling-jet thickness and vertical distribution along flat-ceilinged horizontal tunnel with natural ventilation," *Tunn. Undergr. Sp. Technol.*, vol. 53, pp. 68–77, 2016, doi: 10.1016/j.tust.2015.12.019.

[16] B. Betting, É. Varea, C. Gobin, G. Godard, B. Lecordier, and B. Patte-Rouland, "Experimental and Numerical investigations of the flow characteristics in confined fires," *J. Phys. Conf. Ser.*, vol. 1107, no. 4, 2018, doi: 10.1088/1742-6596/1107/4/042015.

[17] H. Zaidaoui, H. Pretrel, K. Varrall, and O. Vauquelin, "Improvement of Flow Field Characterization in case of Fire Scenario in a Ventilated Compartment with PIV Technique," in *Proceedings of the Tenth International Seminar on Fire and Explosion Hazards, 22-27 May 2022, Oslo, Norway*, 2022.

[18] V. Babrauskas and S. J. Grayson, *Heat release in fires*. Interscience communications, 1990.

[19] B. A. Giannakopoulos, N. B. Kaye, and G. R. Hunt, "The influence of room geometry on the overturning of smoke owing to a floor fire," *Proc. Inst. Civ. Eng. Eng. Comput. Mech.*, vol. 166, no. 2, pp. 68–87, 2013, doi: 10.1680/eacm.9.00005.

[20] N. B. Kaye and G. R. Hunt, "Overturning in a filling box," *J. Fluid Mech.*, vol. 576, pp. 297–323, 2007, doi: 10.1017/S0022112006004435.

[21] H. Pretrel and L. Audouin, “New developments in data regression methods for the characterization of thermal stratification due to fire,” *Fire Saf. J.*, vol. 76, pp. 54–64, 2015, doi: 10.1016/j.firesaf.2015.05.004.

[22] C. L. Beyler, “Fire plumes and ceiling jets,” *Fire Saf. J.*, vol. 11, no. 1–2, pp. 53–75, 1986, doi: 10.1016/0379-7112(86)90052-4.

Figure captions